



HAL
open science

Photoelectron spectrum of the pyridyl radical

Emil Karaev, Marius Gerlach, Katharina Theil, Gustavo Garcia, Christian Alcaraz, Jean-Christophe Loison, Ingo Fischer

► **To cite this version:**

Emil Karaev, Marius Gerlach, Katharina Theil, Gustavo Garcia, Christian Alcaraz, et al.. Photoelectron spectrum of the pyridyl radical. *Physical Chemistry Chemical Physics*, 2024, 26, pp.17042-17047. 10.1039/d4cp00688g . hal-04603509

HAL Id: hal-04603509

<https://hal.science/hal-04603509v1>

Submitted on 6 Jun 2024

HAL is a multi-disciplinary open access archive for the deposit and dissemination of scientific research documents, whether they are published or not. The documents may come from teaching and research institutions in France or abroad, or from public or private research centers.

L'archive ouverte pluridisciplinaire **HAL**, est destinée au dépôt et à la diffusion de documents scientifiques de niveau recherche, publiés ou non, émanant des établissements d'enseignement et de recherche français ou étrangers, des laboratoires publics ou privés.

Cite this: DOI: 00.0000/xxxxxxxxxx

Photoelectron Spectrum of the Pyridyl Radical

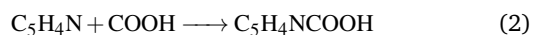
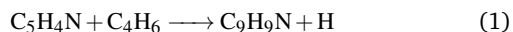
Emil Karaev,^a Marius Gerlach,^a Katharina Theil,^a Gustavo A. Garcia,^b Christian Alcaraz,^c Jean-Christophe Loison,^d and Ingo Fischer^{*a}Received Date
Accepted Date

DOI: 00.0000/xxxxxxxxxx

We report the photoelectron spectrum of the pyridyl radical (C₅H₄N), a species of interest in astrochemistry and combustion. The radicals were produced via hydrogen abstraction in a fluorine discharge and ionized with synchrotron radiation. Mass-selected slow photoelectron spectra of the products were obtained from photoelectron-photoion coincidence spectra. A Franck-Condon simulation based on computed geometries and vibrational frequencies identified contributions of the *o*- and *p*-pyridyl radicals. For the *o*-isomer an adiabatic ionisation energies of 7.70 eV was obtained, in excellent agreement with a computed value of 7.72 eV. The spectrum of *o*-pyridyl is characterized by a long progression in an in-plane bending mode and the N-C stretch that contains the radical site.

1 Introduction

Interest in the pyridyl radical, C₅H₄N is connected to the formation of polycyclic aromatic nitrogen-containing hydrocarbons (PANHs), which are of interest in astrochemistry as potential carriers of the unidentified infrared bands (UIB).^[1] They are also suspected as possible precursors for biomolecules in space, following the discovery of vitamin B3 and nucleobases on meteorites.^[2,4] This motivated researchers to investigate their formation in the gas phase.^[5,7] Nevertheless, little is known so far about their light-induced chemistry. Only recently, the dissociative photoionisation of two PANHs, quinoline and isoquinoline, has been investigated.^[8] The pyridyl radical might be a key intermediate in their formation. For instance, it has been shown that the reaction of pyridyl with 1,3-butadiene (1) leads to derivatives of (iso)quinoline, while a radical-radical recombination of pyridyl with a hydroxycarbonyl radical (2) leads to vitamin B3.^[5,9]



Furthermore, a number of N-containing radicals are included in kinetic models describing the atmospheric chemistry of Titan.^[10] Pyridyl itself can be formed in a high energy environment through photodissociation of a C-H bond in pyridine.^[11] The radi-

cal has been investigated by ESR^[12] and its photodissociation was studied by high-*n* Rydberg atom time of flight spectroscopy^[13]. Rotational spectra have been predicted from high-level coupled cluster calculations.^[14]

N-containing heterocycles are also relevant in combustion of coal and biofuels. During coal burning, fuel-bound nitrogen, which consists mainly of pyrrole and pyridine rings, is oxidized and burned,^[15] and produces CO₂, NO_x as well as HCN.^[15,18] Therefore, reactions of pyrrole and pyridine have been investigated by various experimental^[17,19,30] and computational methods. Generation of pyridyl is often a key step in these reactions.^[28,34] Wu et al. investigated the oxidation reactions of pyridine and found in their kinetic analysis that the major nitrogen-containing oxidation products are HCN, N₂, N₂O, and HNCO.^[30] In pyridine oxidation, the hydrogen abstraction from pyridine to a pyridyl radical by OH (3) is the first step in a cascade of reactions^[30]



In their analysis, Wu et al. only included the lowest energy *o*-pyridyl isomere. However, the *m*- and *p*-isomers are only slightly higher in energy. Table 1 summarizes the relative energies at 298 K of all three isomers and their cations, while figure 1 shows their structures. Although the *o*-pyridyl is the most stable, at combustion temperatures generation of *m*- and *p*-pyridyl is possible. The decomposition pathways of all three isomers have been computed by Cheng and Liu.^[31,35,37] A larger propensity towards small molecule products was found for *m*-pyridyl.

The cations of the pyridyl isomers are also relevant to astrochemistry but, in contrast to the neutral isomers, they have not yet been theoretically investigated. We therefore initiated

^a University of Würzburg, Institute of Physical and Theoretical Chemistry, am Hubland, 97074 Würzburg, Germany

E-mail: ingo.fischer@uni-wuerzburg.de

^b Synchrotron Soleil, L'Orme des Merisiers, St Aubin, B.P. 48, F-91192 Gif sur Yvette, France

^c Université Paris-Saclay, CNRS, Institut de Chimie Physique, UMR8000, 91405 Orsay, France

^d ISM-CNRS, Université de Bordeaux, 351 cours de la Liberation, F-33405 Talence, France

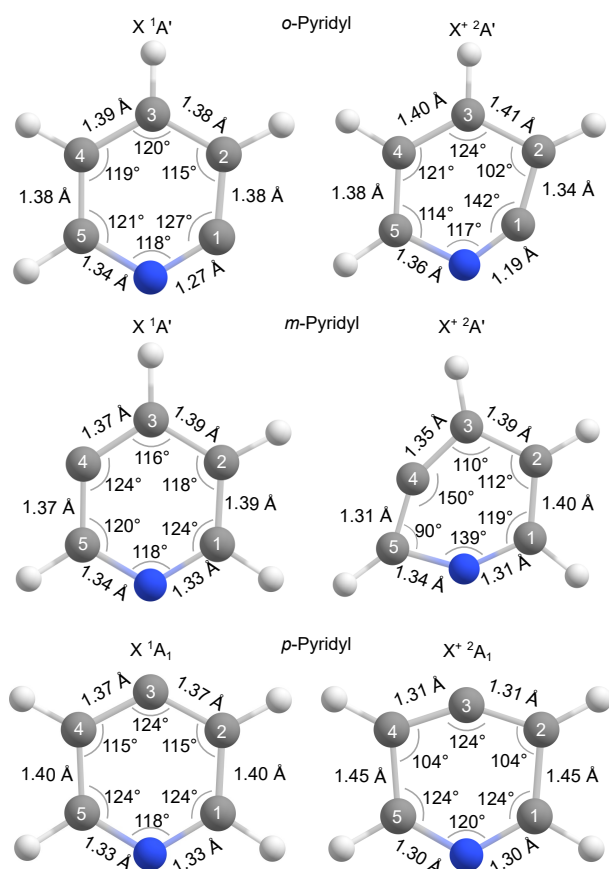


Fig. 1 Calculated geometries of the X^1A' and X^+2A' states of *o*- and *m*-pyridyl and of the X^1A_1 and X^+1A_1 states of *p*-pyridyl. The largest geometric changes from neutral species to cation involve the carbon atom, from which the hydrogen is abstracted. The calculations of the neutrals are in agreement with previous work.¹⁴

an investigation of pyridyl photoionisation using photoelectron-photoion-coincidence (PEPICO) spectroscopy.^{38,39} This method permits recording mass-selected slow photoelectron (ms-SPE) spectra by correlating ions and electrons, and is therefore well suited to investigate radicals as shown previously.^{40,41} In contrast to conventional photoelectron spectroscopy ms-SPE spectra are not perturbed by contributions from precursors or side products, due to photoion mass-selection. The present work continues a program aimed at investigating the photoionisation of N-containing radicals, like NH ⁴², NH_2 ^{43,44}, NF ⁴⁵, NCO ⁴⁶, $HBNH$ ⁴⁷, picolyl⁴⁸, pyrrolyl⁴⁹, 2-azidoacetic acid ($N_3CH_2CO_2H$)⁵⁰ or the anilino radical (C_6H_5NH)⁵¹.

Experimental

The experiments were performed at the DESIRS vacuum ultraviolet (VUV) beamline at the Synchrotron SOLEIL,⁵² using the DELICIOUS III spectrometer.⁵³ The experimental setup has already been published before.^{54,55} In brief, F-atoms were generated in a mixture of 5 % F_2 in Helium using a 2.45 GHz microwave discharge. The product mixture was then transported to a flow tube reactor, where it reacted with 0.5 % gaseous pyri-

Table 1 Relative energies of *o*-, *m*- and *p*-pyridyl and their ionisation energies (IE) for transitions into S_0^+ and T_1^+ .

	method	<i>o</i> -pyridyl	<i>m</i> -pyridyl	<i>p</i> -pyridyl
E_{rel} (neutral)	QCISD(T) ⁶¹	0.00	0.25	0.19
	ω B97X-D3	0.00	0.28	0.21
/ eV	CCSD(T) ¹⁴	0.00	0.24	0.18
$IE_{calc.} / eV (S_0^+)$	ω B97X-D3	7.72	8.33	8.50
	CCSD(T)	7.61	8.78	8.40
$IE_{calc.} / eV (T_1^+)$	ω B97X-D3	9.45	9.39	9.36
$IE_{exp.} / eV$		7.70	–	–

dine diluted in argon, inserted through an injector in the reactor. The reaction mixture passed through two skimmers before being ionized by the monochromatic synchrotron radiation. Electrons and ions are accelerated in opposite directions towards a velocity map imaging detector⁵⁶ and a Wiley-MacLaren time of flight mass spectrometer⁵⁷ that are operated in coincidence. The particles were accelerated with a DC field of 88 V cm^{-1} , which leads to a Stark-shift of roughly 7 meV that was properly taken into account in the determination of ionisation energies. This double imaging PEPICO setup allows filtering the photoelectrons by the corresponding ion's mass, hence removing the contribution from other masses, like the precursor or side products.

Mass-selected photoelectron images of the pyridyl radical (m/z 78) were recorded in the region of 7.6 - 10.2 eV in 5 meV steps. The photoelectron spectra as function of the photon energy constitute a 2D matrix. Since for direct photoionization, the energy of the photoelectrons increases with the photon energy, these 2D spectra consist of a set of parallel lines with constant slope, corresponding to the different cationic levels.⁵⁸ Integration along these lines up to a relative small kinetic energy yields the slow photoelectron spectrum (SPES).^{53,59,60}

To support the experimental interpretation, geometries of the three isomers and their respective cation were optimised and frequencies calculated with ORCA 5.0.3 at the DFT (ω B97x-D3) level using a cc-pVTZ basis set.⁶¹ Single point energies of the optimised structures were also carried out with CCSD(T). The calculated ionisation energies are corrected for the contribution of the zero-point energy. Franck-Condon (FC) factors for ionisation were calculated with ezSpectra⁶² based on the computed geometries and frequencies within the harmonic approximation. The frequencies were scaled by a factor of 0.956 according to the Computational Chemistry Comparison and Benchmark DataBase.⁶³ The resulting stick spectra were convolved with a Gaussian function of 40 meV full width at half maximum height.

Results and Discussion

A fluorine discharge is well suited to synthesize elusive species, but is not very selective. Therefore, a product analysis is presented in Figure 2, which shows the time-of-flight mass spectrum (TOF-ms) recorded at 10.0 eV photon energy. The main contribution is pyridine C_5H_5N with m/z 79 and its ^{13}C isotope m/z 80. In addition to the single hydrogen abstraction at m/z 78, double abstraction can be deduced from the peak at m/z 77. Although

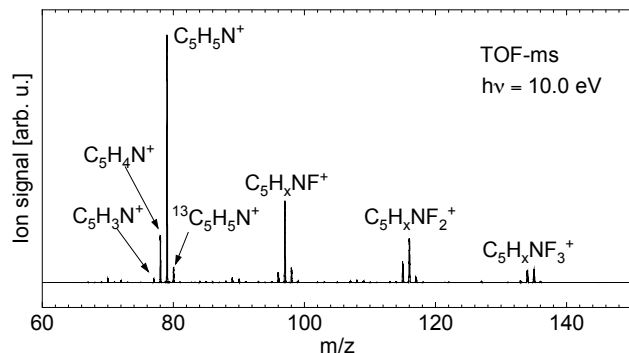


Fig. 2 Time of Flight mass spectrum (TOF-MS) at 10.0 eV photon energy. The precursor pyridine is observed at m/z 79. Besides the target $C_5H_4N^+$ (m/z 78) a small amount of doubly dehydrogenated $C_5H_3N^+$ (m/z 77) is visible. At higher m/z also fluorinated species are detected.

m/z 76 is not detected, the observation of m/z 134 ($C_5H_2NF_3^+$) suggests a possible third abstraction. F-atom addition products are responsible for the peaks at m/z 96 - 98, 115 - 117 and 134, 135, showing the addition of one to three fluorine atoms to the aromatic ring.

As noted above, hydrogen abstraction from pyridine leads to three possible cyclic isomers, *o*-, *m*-, and *p*-pyridyl, depending on which hydrogen is cleaved. However, from each isomer a reaction pathway to a stable open chain structure is available, which has to be taken into account in the assignments. The lowest energy barriers to ring opening are 1.75 eV, 1.98 and 2.68 eV for the *o*-, *m*-, and *p*-isomer, respectively.^{31,35,37,64} The heat of reaction $\Delta_r H^\circ$ for (4) at 298 K ranges from 0.8 to 1.1 eV depending on the isomer.



Thus ring opening requires additional collisions in the reactor. Although this is certainly possible, open chain species of m/z 78 were not observed, either because the IE is not in the investigated energy range or the contribution of open chain isomers to m/z 78 is relatively small compared to the cyclic isomers. IE's of several low-energy open chain isomers³¹ were also computed. The values are summarized in Table S1 in the electronic supplementary information (ESI).

The slow photoelectron spectrum (SPES) of m/z 78 in the range from 7.6 - 9.5 eV is given in Figure 3. Trace a) shows the experimental spectrum. The first band appears at 7.70 eV, followed by a progression up to 8.6 eV with a spacing of around 630 cm^{-1} . Above 8.6 eV, a second band system appears, without discernible structure. Trace b) depicts the Franck-Condon (FC) simulation of the lowest energy *o*-pyridyl isomer in blue, based on the geometries shown in Figure 1, which were calculated on a DFT level. The bond lengths and angles differ by a maximum of 0.01 \AA and 4° , compared to the CCSD(T) optimisation of Meyer et al.¹⁴ Taking the FWHM of bands into account, the IE of the $X^+ 1A' \leftarrow X^2A'$ transition is determined to be $7.70 \pm$

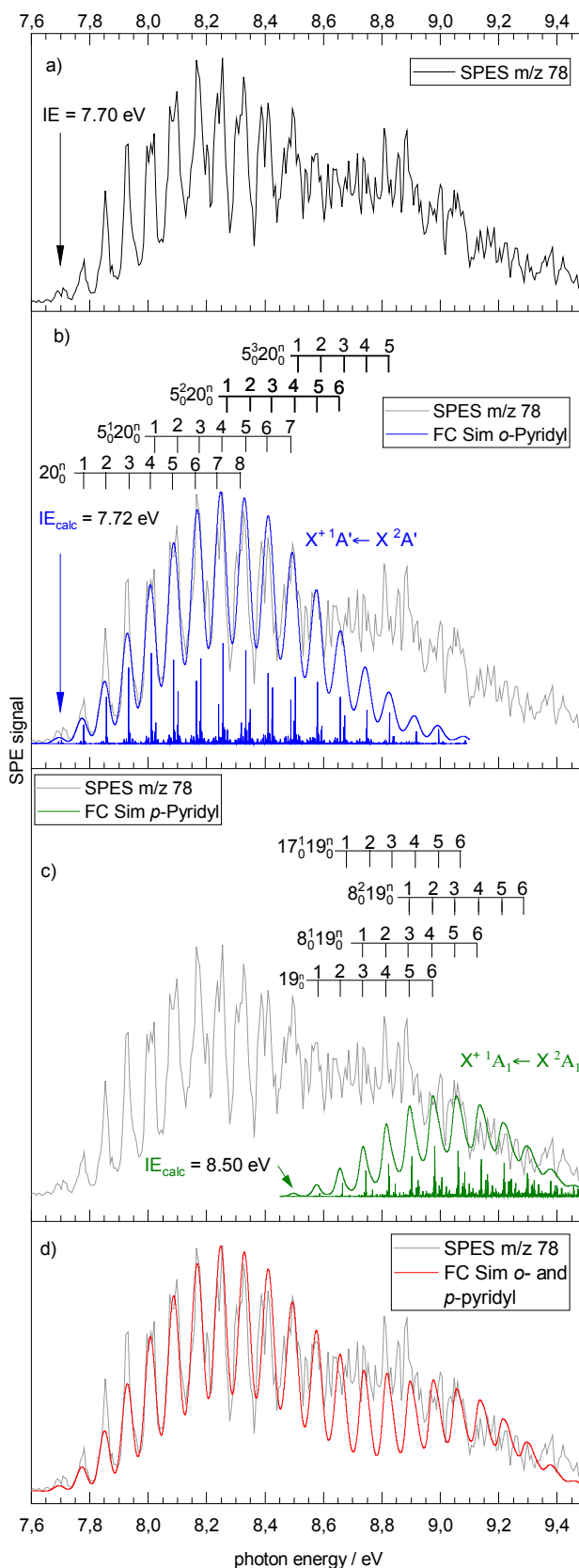


Fig. 3 a) SPES of m/z 78 recorded from 7.60 - 9.5 eV. b) The blue simulation shows the $X^+ 1A' \leftarrow X^2A'$ transition of the *o*-pyridyl isomer. The calculated ionisation energy is 7.72 eV. c) The green simulation describes the $X^+ 1A_1 \leftarrow X^2A_1$ transition of *p*-pyridyl. Its calculated ionisation energy lies at 8.50 eV. d) The red simulation is a sum of the simulations in b) and c) with a ratio of 1 : 0.4.

0.020 eV. The calculated IE is 7.72 eV for ω B97X-D3 and 7.61 eV for CCSD(T) and is in agreement with the experimental IE. The long progression is due to a large geometry change upon ionisation, as can be derived from Figure 1. The largest changes involve the NC₁ bond length (C₁ being the radical site) that shortens by 0.8 Å upon ionisation and the N-C₁-C₂ bond angle that is reduced by 15°. This results in a pronounced progression of the N-C₁-C₂ bending mode ν_{20}^+ , with a computed wavenumber of $\nu_{20}^+ = 640 \text{ cm}^{-1}$ (80 meV). This frequency corresponds well with the experimental spacing of 630 cm^{-1} and confirms the assignment. The mode also appears in combination with the fundamental and first as well as second overtone of the NC₁ stretching mode ν_5^+ , with a wavenumber of $\nu_5^+ = 2000 \text{ cm}^{-1}$ (250 meV).

Low-lying triplet states might be relevant in the photoionisation of pyridyl isomers, therefore the IEs of the (T_1^+) states have also been calculated and their values are given in table 4. As visible, transitions into the triplet cations are only expected above 9.36 eV. In fact, a band at higher photon energies (see Figure S1 in the ESI) is assigned to the (T_1^+) states. However, there is no indication that the triplet cations play a role in the spectral region shown in Figure 3.

As visible, the simulation of the $X^+ \ ^1A' \leftarrow X \ ^2A'$ transition of *o*-pyridyl matches the low-energy part of the spectrum quite well. However, the high-energy part of the spectrum is not represented well, which suggests a contribution by another isomer. Trace c) shows the simulation of the $X^+ \ ^1A_1 \leftarrow X \ ^2A_1$ transition of the *p*-pyridyl isomer in green, based on the computed IE of 8.50 eV. The overall signal intensity at higher energies is matched well. In Figure 1 one can see, that the main change in geometry upon ionisation is due to the C₁-C₂-C₃/C₅-C₄-C₃ angle, which is reduced by 11°, and the C₂-C₃/C₄-C₃ bond, which shortens by 0.06 Å. This leads to a progression in three modes and their combination bands, a C₂-C₃-C₄ bending mode $\nu_{19}^+ = 660 \text{ cm}^{-1}$, a C₁-N-C₅ bending mode $\nu_{17}^+ = 860 \text{ cm}^{-1}$ and a C₁-C₂/C₅-C₄ stretching mode $\nu_8^+ = 1340 \text{ cm}^{-1}$. However, the modes cannot be distinguished in the experimental spectrum. The neutral geometry on the DFT level of *p*-pyridyl is in agreement with the CCSD(T) geometry.¹⁴ The bond lengths differ by a maximum of 0.005 Å and the bond angles by a maximum of 1°.

In trace d) the simulations of *o*-, and *p*-isomer are combined, the total simulated intensity is given as a red line. Assuming that the ionisation cross sections are the same for all isomers, FC simulations of the electron signal can then provide a quantitative isomer ratio. The best agreement with the experimental spectrum is achieved with an *o*- to *p*-ratio of 1 : 0.4. In a thermal equilibrium at room temperature an *p*-/*o*-ratio of 1:1000 would be expected. The contribution of *m*-pyridyl would even be another factor of 10 smaller.

Given the non-Boltzmann isomer ratio, the small remaining deviation from 8.5 eV to 8.9 eV between experiment and simulation might be due to contributions of *m*-pyridyl, whose calculated IE

lies at 8.33 eV on the DFT level and at 8.78 eV in CCSD(T) calculations. As product formation is governed by the H-abstraction kinetics and preliminary calculations indicate a difference of only 20 meV between the transition states leading to the various product isomers, *m*-pyridyl would indeed be expected to be formed as well. However, as visible in the center trace of Figure 1, the geometry change upon photoionization is larger than for *o*- and *p*-pyridyl and a significant deformation of the ring is visible in the cation of the *m*-isomer. This leads to very small FC-factors close to the ionisation threshold and a small contribution of *m*-pyridyl to the SPES-spectrum, cf. Figure 3, which is neglected in the simulation. In addition, transitions into the excited triplet state of the open chain cations might also show small contributions at higher energies. As visible in Figure S1 in the ESI, it is difficult to extract information on possible small contributions of other isomers to the spectrum.

Conclusion

We recorded a mass-selected photoelectron spectrum of the pyridyl radical using photoelectron-photoion coincidence spectroscopy. Pyridyl was produced from pyridine in a fluorine discharge. The spectrum is dominated by the *o*-pyridyl isomer. An ionisation energy of 7.70 eV was determined, in good agreement with the calculated value of 7.72 eV. A large geometry change upon ionisation leads to a long progression in an in-plane bending mode and a N-C stretch that includes the radical site. Even though *o*-pyridyl is the most stable isomer, an estimated 29 % of *p*-pyridyl is also present. Its photoionisation was found to contribute to the high-energy part of the spectrum. An IE of 8.50 eV was computed. The *m*-isomer on the other hand contributes only negligibly to the spectrum, likely due to low FC factors.

While the neutral species maintain a pyridine-like structure, the cations show a significant deformation of the ring. In the case of *o*-pyridyl, this leads to a long progression in the N-C₁ stretching mode ν_5^+ and the N-C₁-C₂ in-plane bending mode ν_{20}^+ . The *p*-pyridyl on the other hand, shows a progression consisting of the C₂-C₃-C₄ bending mode ν_{19}^+ , the C₁-N-C₅ bending mode ν_{17}^+ and the C₁-C₂ stretching mode ν_8^+ . Open chain isomers with the same *m/z* as pyridyl were not detected.

Acknowledgements

This work was performed on the DESIRS beamline under Proposal No. 20210362. We acknowledge SOLEIL for provision of synchrotron radiation facilities and the DESIRS beamline team for their assistance. The work was supported by the Deutsche Forschungsgemeinschaft, FI575/13-2. JCL and GAG acknowledge financial contribution from the Agence National de la Recherche (ANR) through the ZEPHIRS project (contract number ANR-21-CE29-0017). We would like to thank D. Schaffner for her support in the experiments.

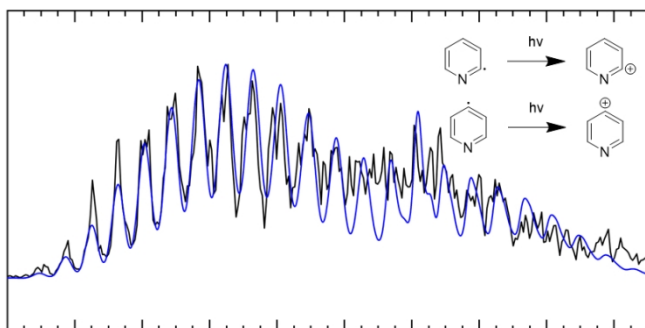
Conflict of Interest

There are no conflicts of interest to declare.

Notes and references

- 1 D. M. Hudgins, C. W. Bauschlicher Jr and L. Allamandola, *ApJ*, 2005, **632**, 316.
- 2 K. E. Smith, M. P. Callahan, P. A. Gerakines, J. P. Dworkin and C. H. House, *Geochim. Cosmochim. Acta*, 2014, **136**, 1–12.
- 3 M. P. Callahan, K. E. Smith, H. J. Cleaves, J. Ruzicka, J. C. Stern, D. P. Glavin, C. H. House and J. P. Dworkin, *Proc. Natl. Acad. Sci.*, 2011, **108**, 13995–13998.
- 4 Z. Martins, O. Botta, M. L. Fogel, M. A. Sephton, D. P. Glavin, J. S. Watson, J. P. Dworkin, A. W. Schwartz and P. Ehrenfreund, *Earth Planet. Sci. Lett.*, 2008, **270**, 130–136.
- 5 D. N. S. Parker and R. I. Kaiser, *Chem. Soc. Rev.*, 2017, **46**, 452–463.
- 6 D. S. N. Parker, R. I. Kaiser, O. Kostko, T. P. Troy, M. Ahmed, A. M. Mebel and A. G. G. M. Tielens, *The Astrophysical Journal*, 2015, **803**, 53.
- 7 J. Bouwman, A. Bodi and P. Hemberger, *Phys. Chem. Chem. Phys.*, 2018, **20**, 29910–29917.
- 8 J. Bouwman, B. Sztaray, J. Oomens, P. Hemberger and A. Bodi, *J. Phys. Chem. A*, 2015, **119**, 1127–1136.
- 9 B. M. McMurtry, A. M. Turner, S. E. Saito and R. I. Kaiser, *Chem. Phys.*, 2016, **472**, 173–184.
- 10 K. Willacy, M. Allen and Y. Yung, *ApJ*, 2016, **829**, 79.
- 11 M.-F. Lin, Y. A. Dyakov, C.-M. Tseng, A. M. Mebel, S. Hsien Lin, Y. T. Lee and C.-K. Ni, *J. Chem. Phys.*, 2005, **123**, 054309.
- 12 D. M. J. Paul H. Kasai, *J. Am. Chem. Soc.*, 1972, **94**, 720–727.
- 13 M. Lucas, J. Minor, J. Zhang and C. Brazier, *J. Phys. Chem. A*, 2013, **117**, 12138–12145.
- 14 K. S. Meyer, J. H. Westerfield, S. L. Johansen, J. Keane, A. C. Wannemacher and K. N. Crabtree, *J. Phys. Chem. A*, 2022, **126**, 3185–3197.
- 15 P. Glarborg, A. Jensen and J. Johnsson, *Prog. Energy Combust. Sci.*, 2003, **29**, 89–113.
- 16 M. A. Wójtowicz, J. R. Pels and J. A. Moulijn, *Fuel*, 1995, **74**, 507–516.
- 17 J. C. Mackie, M. B. Colket III, P. F. Nelson and M. Esler, *Int. J. Chem. Kinet.*, 1991, **23**, 733–760.
- 18 Z.-Y. Zhao, F. Cao, M.-Y. Fan, W.-Q. Zhang, X.-Y. Zhai, Q. Wang and Y.-L. Zhang, *Atmos. Environ.*, 2020, **242**, 117762.
- 19 Z. Tian, Y. Li, T. Zhang, A. Zhu, Z. Cui and F. Qi, *Combust. Flame.*, 2007, **151**, 347–365.
- 20 Z. Tian, Y. Li, T. Zhang, A. Zhu and F. Qi, *J. Phys. Chem. A*, 2008, **112**, 13549–13555.
- 21 J. C. Mackie, M. B. Colket and P. F. Nelson, *J. Phys. Chem.*, 1990, **94**, 4099–4106.
- 22 J. MacNamara and J. Simmie, *Combust. Flame.*, 2003, **133**, 231–239.
- 23 A. T. M. U. Alzueta and R. Bilbao, *Combust. Sci. Technol.*, 2002, **174**, 151–169.
- 24 T. Yamamoto, T. Kuwahara, K. Nakaso and T. Yamamoto, *Fuel*, 2012, **93**, 213–220.
- 25 X. J. Chang'an Wang, Yongbo Du and D. Che, *Energ. Source. Part A*, 2016, **38**, 975–981.
- 26 B. Chen, P. Liu, M. Pelucchi, C. Guidici, L. P. Maffei, S. Faller, Q. Xu, J. Huang, F. Zhang, C. Huang, K. Leonhard, Z. Wang, M. Mehl, W. L. Roberts, T. Faravelli and H. Pitsch, *Proc. Combust. Inst.*, 2023, **39**, 73–84.
- 27 M. Pelucchi, S. Arunthanayothin, Y. Song, O. Herbinet, A. Stagni, H.-H. Carstensen, T. Faravelli and F. Battin-Leclerc, *Energy Fuels*, 2021, **35**, 7265–7284.
- 28 X. Hong, L. Zhang, T. Zhang and F. Qi, *J. Phys. Chem. A*, 2009, **113**, 5397–5405.
- 29 L.-N. Wu, Z.-Y. Tian, J.-J. Weng, D. Yu, Y.-X. Liu, D.-X. Tian, C.-C. Cao, J.-B. Zou, Y. Zhang and J.-Z. Yang, *Combust. Flame.*, 2019, **202**, 394–404.
- 30 L.-N. Wu, Z.-Y. Tian, K.-R. Jin, Z.-H. Zheng, D. Wang, B.-Z. Liu, Q. Xu and Z.-D. Wang, *Combust. Flame.*, 2022, **243**, 112042.
- 31 R. Liu, T. T.-S. Huang, J. Tittle and D. Xia, *J. Phys. Chem. A*, 2000, **104**, 8368–8374.
- 32 J. Liu and X. Guo, *Fuel Process. Technol.*, 2017, **161**, 107–115.
- 33 Y. Ninomiya, Z. Dong, Y. Suzuki and J. Koketsu, *Fuel*, 2000, **79**, 449–457.
- 34 T. Jiao, H. Fan, S. Liu, S. Yang, W. Du, P. Shi, C. Yang, Y. Wang and J. Shangguan, *Chin. J. Chem. Eng.*, 2021, **35**, 107–123.
- 35 X. L. Cheng, Y. Y. Zhao and Z. Y. Zhou, *J. Mol. Struct.*, 2004, **678**, 17–21.
- 36 X. Cheng, *J. Mol. Struct.*, 2005, **731**, 89–99.
- 37 X. Cheng, L. Niu, Y. Zhao and Z. Zhou, *Spectrochim. Acta A*, 2004, **60**, 907–914.
- 38 T. Baer and R. P. Tuckett, *Phys. Chem. Chem. Phys.*, 2017, **19**, 9698–9723.
- 39 J. M. Dyke, *Physical Chemistry Chemical Physics*, 2019, **21**, 9106–9136.
- 40 I. Fischer and S. T. Pratt, *Physical Chemistry Chemical Physics*, 2022, **24**, 1944–1959.
- 41 I. Fischer and P. Hemberger, *ChemPhysChem*, 2023, e202300334.
- 42 G. A. Garcia, B. Gans, X. Tang, M. Ward, S. Batut, L. Nahon, C. Fittschen and J.-C. Loison, *Journal of Electron Spectroscopy and Related Phenomena*, 2015, **203**, 25–30.
- 43 F. Holzmeier, M. Lang, I. Fischer, P. Hemberger, G. Garcia, X. Tang and J.-C. Loison, *Physical Chemistry Chemical Physics*, 2015, **17**, 19507–19514.
- 44 S. Dunlavey, J. Dyke, N. Jonathan and A. Morris, *Molecular Physics*, 1980, **39**, 1121–1135.
- 45 J. M. Dyke, N. Jonathan, A. E. Lewis and A. Morris, *Journal of the Chemical Society, Faraday Transactions 2: Molecular and Chemical Physics*, 1982, **78**, 1445–1450.
- 46 J. Dyke, N. Jonathan, A. Lewis, J. Mills and A. Morris, *Molecular Physics*, 1983, **50**, 77–89.
- 47 D. Schleier, D. Schaffner, M. Gerlach, P. Hemberger and I. Fischer, *Phys. Chem. Chem. Phys.*, 2022, **24**, 20–24.
- 48 E. Reusch, F. Holzmeier, M. Gerlach, I. Fischer and P. Hemberger, *Chemistry—A European Journal*, 2019, **25**, 16652–16659.
- 49 F. Holzmeier, I. Wagner, I. Fischer, A. Bodi and P. Hemberger, *The Journal of Physical Chemistry A*, 2016, **120**, 4702–4710.

- 50 J. Dyke, A. Groves, A. Morris, J. Ogden, A. Dias, A. Oliveira, M. Costa, M. Barros, M. Cabral and A. Moutinho, *Journal of the American Chemical Society*, 1997, **119**, 6883–6887.
- 51 H. R. Hrodmarsson, G. A. Garcia, L. Nahon, B. Gans and J.-C. Loison, *The Journal of Physical Chemistry A*, 2019, **123**, 9193–9198.
- 52 L. Nahon, N. de Oliveira, G. A. Garcia, J.-F. Gil, B. Pilette, O. Marcouillé, B. Lagarde and F. Polack, *J. Synchrotron Rad.*, 2012, **19**, 508–520.
- 53 G. A. Garcia, B. K. Cunha de Miranda, M. Tia, S. Daly and L. Nahon, *Rev. Sci. Instrum.*, 2013, **84**, 069902.
- 54 G. A. Garcia, B. Gans, X. Tang, M. Ward, S. Batut, L. Nahon, C. Fittschen and J.-C. Loison, *J. Electron Spectrosc. Relat. Phenom.*, 2015, **203**, 25–30.
- 55 G. A. Garcia, X. Tang, J.-F. Gil, L. Nahon, M. Ward, S. Batut, C. Fittschen, C. A. Taatjes, D. L. Osborn and J.-C. Loison, *J. Chem. Phys.*, 2015, **142**, 164201.
- 56 D. H. Parker and A. T. J. B. Eppink, *J. Chem. Phys.*, 1997, **107**, 2357–2362.
- 57 W. C. Wiley and I. H. McLaren, *Rev. Sci. Instrum.*, 1955, **26**, 1150–1157.
- 58 G. A. Garcia, L. Nahon and I. Powis, *Rev. Sci. Instrum.*, 2004, **75**, 4989–4996.
- 59 G. A. Garcia, H. Soldi-Lose and L. Nahon, *Review of Scientific Instruments*, 2009, **80**, 023102.
- 60 J. Pouilly, J. Schermann, N. Nieuwjaer, F. Lecomte, G. Gregoire, C. Desfrancois, G. Garcia, L. Nahon, D. Nandi, L. Poisson *et al.*, *Physical Chemistry Chemical Physics*, 2010, **12**, 3566–3572.
- 61 F. Neese, F. Wennmohs, U. Becker and C. Riplinger, *J. Chem. Phys.*, 2020, **152**, 224108.
- 62 S. Gozem and A. I. Krylov, *Wiley Interdiscip. Rev. Comput. Mol. Sci.*, 2022, **12**, e1546.
- 63 R. D. Jhonson, *Computational Chemistry Comparison and Benchmark DataBase*, 2022.
- 64 F. Tureček, J. K. Wolken and M. Sadílek, *Eur. J. Mass Spectrom.*, 1998, **4**, 321–332.



855x481mm (38 x 38 DPI)

Electronic Supplementary Information for
Photoelectron Spectrum of the Pyridyl Radical

Emil Karaev,^a Marius Gerlach,^a Katharina Theil,^a Gustavo A. Garcia,^b Christian Alcaraz,^c
Jean-Christophe Loison,^d and Ingo Fischer*^a

^a Institute of Physical and Theoretical Chemistry, University of Würzburg, Am Hubland,
97074 Würzburg, Germany. E-mail: ingo.fischer@uni-wuerzburg.de.

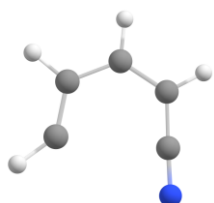
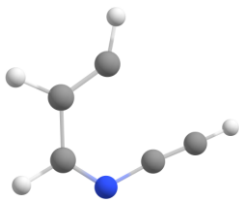
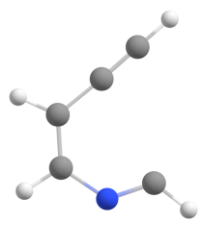
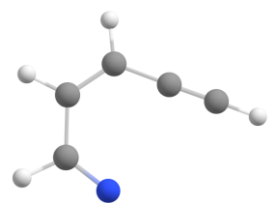
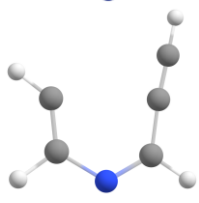
^b Synchrotron Soleil, L'Orme des Merisiers, St Aubin, B.P. 48, F-91192 Gif sur Yvette,
France.

^c Université Paris-Saclay, CNRS, Institut de Chimie Physique, UMR8000, 91405 Orsay,
France

^d ISM-CNRS, Université de Bordeaux, 351 cours de la Libération, F-33405 Talence,
France

	Page
Calculated ionisation energies for the open shell <i>isomers</i>	S2
SPES of $m/z = 78$ from 9.5 – 10.2 eV	S3
Reference	S3

Table S1: Calculated ionisation energies for the open shell isomers suggested by Liu et al.^[1]

	Open shell isomer	$IE_{\text{calc.}}(S_0^+)/\text{eV}$	$IE_{\text{calc.}}(T_1^+)/\text{eV}$
1		6.10	9.11 eV
2		4.42	8.47
3		no convergence	8.35
4		6.45	8.98
5		5.20	8.19

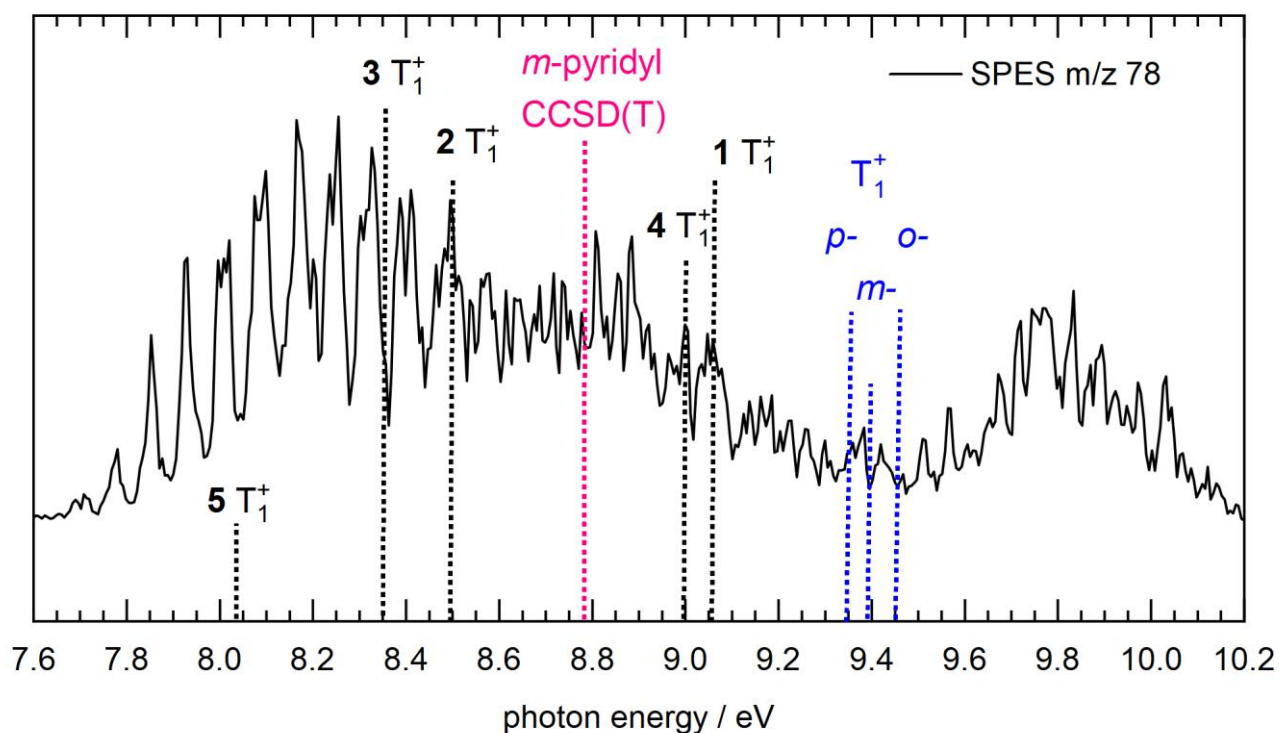


Fig. S1: SPES of $m/z = 78$ from 9.5 – 10.2 eV. The IE of *m*-pyridyl, computed by CCSD(T) is given as a purple line. For comparison the computed IEs for transitions into the triplet cation of the open-chain isomers are given as black lines. A second band starting at 9.6 eV is most likely due to transitions into the triplet states of the pyridyl cations. Due to the close-lying ionization energies, an identification of further isomers in addition to *o*- and *p*-pyridyl is not possible.

Notes and references

[1]: R. Liu, T. T.-S. Huang, J. Tittle and D. Xia, *J. Phys. Chem. A*, 2000, **104**, 8368–8374.